ELSEVIER

Thermochimica Acta 256 (1995) 213–226

thermochimica acta

Evaluation of water in silica pores using differential scanning calorimetry

K. Ishikiriyama*, M. Todoki

Toray Research Center, Inc., Material Characterization Laboratories, 3-7 Sonoyama 3-Chome, Otsu, Shiga 520, Japan

Received 25 July 1994; accepted 1 November 1994

Abstract

The state of water confined in the pores of commercial silica gels has been investigated as a function of the water content using differential scanning calorimetry (DSC). There were at least two kinds of water present: freezable pore water and nonfreezable pore water. The amounts of these types of water were precisely determined as a function of total water content using the temperature dependence of the heat of melting of pore ice due to the melting temperature distribution. In all the silica gels, an endothermic peak of freezable pore water appeared after the nonfreezable pore water content was saturated, and then an endothermic peak of bulk water overflowing the silica gel appeared after both freezable and nonfreezable pore water content was saturated. The thicknesses of the layers of nonfreezable pore water were estimated to be 0.4–0.8 nm, which corresponds to two or three monolayers of water. Considering the densities of the various types of water, the pore volumes were also calculated from the DSC curves and were found to be in good agreement with those obtained using nitrogen gas adsorption–desorption. By using the average densities of water, the densities of freezable and nonfreezable pore water were estimated to be similar to those of bulk water and bulk ice, respectively.

Keywords: DSC; Non-freezable water; Silica gel; Pore volume; Pore water

1. Introduction

A melting temperature depression of ice confined in pores was predicted by Belorai and Bylina [1], and indeed such behavior has been observed for both

* Corresponding author.

0040-6031/95/$09.50 © 1995 – Elsevier Science B.V. All rights reserved
SSDI 0040-6031(94)02174-0

benzene and water in silica gels [2,3]. Earlier studies on the structure of water near solid interfaces have been reviewed by Drost-Hansen [4]. Rennie and Clifford investigated the melting of ice in porous silica using differential scanning calorimetry (DSC) and nuclear magnetic resonance (NMR) [5], and they concluded that water in the pores has essentially bulk properties at distances of > 1 nm from the surface. In contrast, Drost-Hansen and Etzler concluded that liquid water confined in silica pores is different from bulk water by measuring the melting of ice in the silica pores [6]. In addition, Handa et al. [7] carried out investigations of the melting of ice in porous Vycor glass and various silica gels using calorimetry and X-ray diffraction, and they concluded that the heat of melting of pore ice was 16–48% smaller than that of bulk ice. As for the melting behavior of some organic materials confined in pores, Jackson and McKenna have reported that the melting temperature of controlled porous glasses with pore radii in the range 4–73 nm decreased with decreasing pore diameter,and a large reduction in the bulk enthalpy of fusion was observed [8].

Although many studies of water confined in pores have been reported, the state of the water confined in the pores was not necessarily clarified. In this paper, a method for precisely determining freezable and nonfreezable pore water is proposed, based on dividing the DSC curves into the heat of melting ice as a function of temperature, which is due to the distribution of the melting temperature according to the distribution of the pore sizes. On the basis of the determination, the properties of the types of water in silica pores are examined from the standpoint of the pore volume, the densities of the water and the thickness of the nonfreezable water layer. This study was carried out as part of a previous investigation to establish a new method [9,10] for determining the pore size distribution from the distribution of melting and freezing temperatures.

2. Experimental

2.1. Sample preparation

Porous silica gels with pore radii in the range 1.8–7.5 nm were obtained from Aldrich Chemical Company and Wako Pure Chemical Industries. Five types of silica gel were used with the following characteristics as provided by the manufacturer: SA18 (Aldrich, 24217-9) with an average pore diameter of 4.0 nm, a pore volume of 0.68 $cm^3\ g^{-1}$ and a surface area of 675 $m^2\ g^{-1}$; SA27 (Aldrich, 28862-4) with an average pore diameter of 6.0 nm, a pore volume of 0.75 $cm^3\ g^{-1}$ and a surface area of $\approx 500\ m^2\ g^{-1}$; SA75 (Aldrich, 23683-7) with average pore diameter 15.0 nm, a pore volume of 0.75 $cm^3\ g^{-1}$ and a surface area of 300 $m^2\ g^{-1}$; SW27 (Wako, 5SIL) with an average pore diameter of 6.0 nm, a pore volume of 0.75 $cm^3\ g^{-1}$ and a surface area of 500 $m^2\ g^{-1}$; SW60 (Wako, 5SIL120) with an average pore diameter of 12.0 nm, a pore volume of 1.0 $cm^3\ g^{-1}$ and a surface area of 300 $m^2\ g^{-1}$.

Samples containing water were prepared by first immersing the silica gels in distilled, deionized water (Wako) and then maintaining the system under reduced pressure with an aspirator for more than 12 h to fill the pores in the silica gel with water. The water contents W_t of the samples, which were prepared by allowing water to escape from the saturated samples by slow evaporation at room temperature and monitoring the mass of the sample, ranged from 0 to 2.6 g of H_2O per g of dry silica gel. After attainment of a given water content, ≈ 10–20 mg of the sample was hermetically sealed in a high-pressure aluminum crucible covered with aluminum oxide on the surface to avoid entirely the reaction of water with aluminum.

2.2. Measurements

A Perkin-Elmer differential calorimeter model DSC-II, equipped with a cooling apparatus and with a data processing system developed by the authors, was used to measure the melting curves of ice in the silica gels. All DSC measurements were carried out over the temperature range 233–283 K at a low scanning rate, 0.31 K min^{-1}, to avoid thermal and time delays in the DSC curve. The accuracy of the heat flux was estimated to be $\approx \pm 3\%$ or better.

At the end of each DSC measurement, a small hole was made in the crucible and it was then dried under vacuum in an oven at 383 K to determine the mass of the water.

All calculations of water content and pore volume, etc., were carried out using a new computer program, which was executed on Windows 3.1 and was written by the authors using Microsoft C compiler and System Development Kits for Windows.

In addition, a BELSORP 36 system (Nihon Bel), which is a device for nitrogen gas adsorption–desorption measurement, was used for characterizing pore size distributions of the dry silica gels and for checking the nominal characteristics.

3. Results and discussion

3.1. DSC curves of water in silica pores

The DSC heating scans for silica gels filled with water are shown in Fig. 1. Two distinct endothermic peaks are to be found in each DSC curve. Although the peak on the high temperature side is located above 273 K, this peak is not due to the melting temperature elevation of water in silica pores. It has been suggested by Drost-Hansen [5] that melting at elevated temperatures in silica might be due to negative pressures resulting from the presence of menisci at the pore openings; however, as the heating rate decreases, the melting peak temperature of the water approaches 273 K and the width of the melting peak tends towards zero. Accordingly, the peak on the high temperature side is assigned to the melting of bulk ice outside the silica gel.

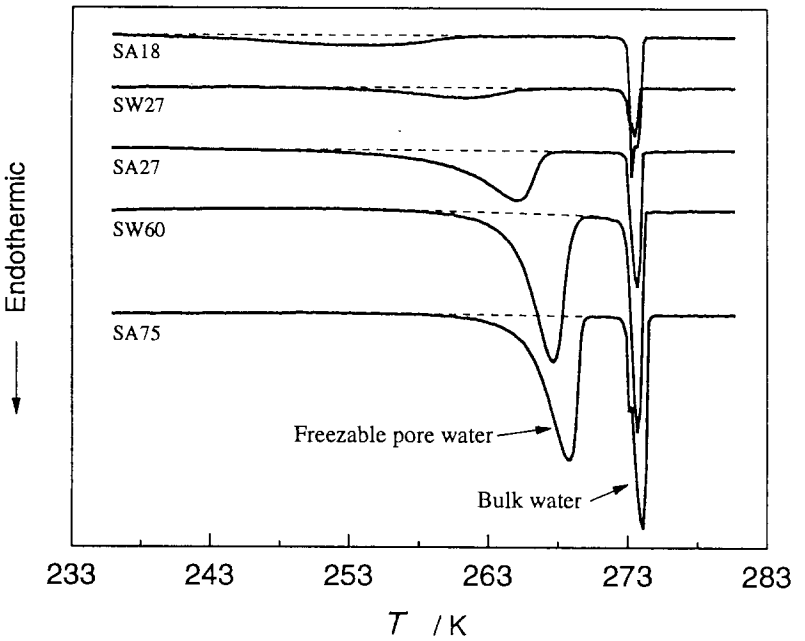

Fig. 1. DSC heating curves of silica gels filled with water. The total water contents are 1.065 (SA18), 0.934 (SA27), 1.602 (SA75), 1.144 (SW27) and 1.595 (SW60) g of water per g of silica gel.

The peak on the low temperature side is assigned to the melting of ice inside the silica pores for the following reason. The assignment of the low temperature endotherm was performed by examination of the relationship between the pore radius of the silica gel and the reciprocal melting peak temperature depression. Table 1 shows peak radii of pore size distribution, surface areas and pore volumes of the silica gels which were obtained by means of nitrogen gas adsorption–desorption using a technique established by Dollimore and Heal [11]. In any silica gel, the nominal pore radii of the gel as noted above are found to be consistent with the peak pore radii in Table 2, $R_{p_{gas}}$, and hence the $R_{p_{gas}}$ can be reasonably compared with the reciprocal melting temperature depression $1/\Delta T_p$. As a result, because an approximately linear relationship exists between $R_{p_{gas}}$ and $1/\Delta T_p$ as shown in Fig. 2,

Table 1
Textural characteristics of silica gels measured using nitrogen gas adsorption – desorption

Sample	$R_{nominal}$/nm	$R_{p_{gas}}$/nm	$V_{p_{gas}}$/cm^3 g^{-1}	$S_{p_{gas}}$/m^2 g^{-1}
SA18	2.0	1.82	0.623	794.0
SA27	3.0	2.73	0.787	602.7
SA75	7.5	7.50	1.256	375.6
SW27	3.0	2.73	1.037	734.4
SW60	6.0	6.00	1.150	384.0

Table 2
Some experimental results obtained with DSC measurements

Sample	T_p[a]/ K	W_{fp}/ g H_2O/g silica gel	W_{nf}/ g H_2O/g silica gel	V_{fp}/ $cm^3\,g^{-1}$	V_{nf}/ $cm^3\,g^{-1}$	V_{Pdsc}[b]/ $cm^3\,g^{-1}$	$\rho_{average}$/ $cm^3\,g^{-1}$	β/nm	
								$z=2$	$z=3$
SA18	254.6	0.197	0.380	0.222	0.415	0.630	0.956	0.76	0.55
SA27	262.7	0.487	0.251	0.548	0.274	0.822	0.972	0.51	0.35
SA75	268.9	0.934	0.176	1.051	0.192	1.243	0.987	0.62	0.42
SW27	261.5	0.476	0.388	0.535	0.424	0.959	0.963	0.70	0.49
SW60	267.9	0.797	0.191	0.897	0.208	1.105	0.984	0.61	0.41

[a] T_p is the melting peak temperature of freezable water. [b] V_{Pdsc} is the pore volume circulated from Eqs. (5) and (8)–(10).

the Kelvin equation can be set up for the system. Consequently, the water with depressed melting point in the silica gels is assigned to the freezable pore water, for which the melting temperature is lower than that of bulk ice owing to the ice–water interfacial tension generated in the pores. The transformation of melting and freezing curves of pore water into pore size distribution curves in silica gels will be described in detail in separate papers [9,10].

The DSC heating curves of water in SW27 are shown in Fig. 3 as a function of total water content. As for SW27, a DSC endothermic peak no longer appears at < 0.2 g of H_2O per g of silica gel. This suggests that the water in the silica gel at

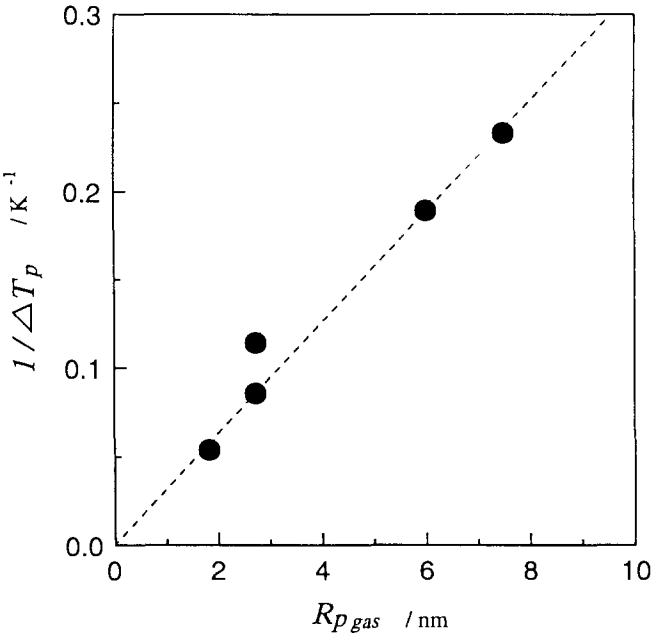

Fig. 2. Relationship between pore radius R_{Pgas} obtained using nitrogen gas adsorption–desorption and the reciprocal of the melting peak temperature depression $1/\Delta T_p$.

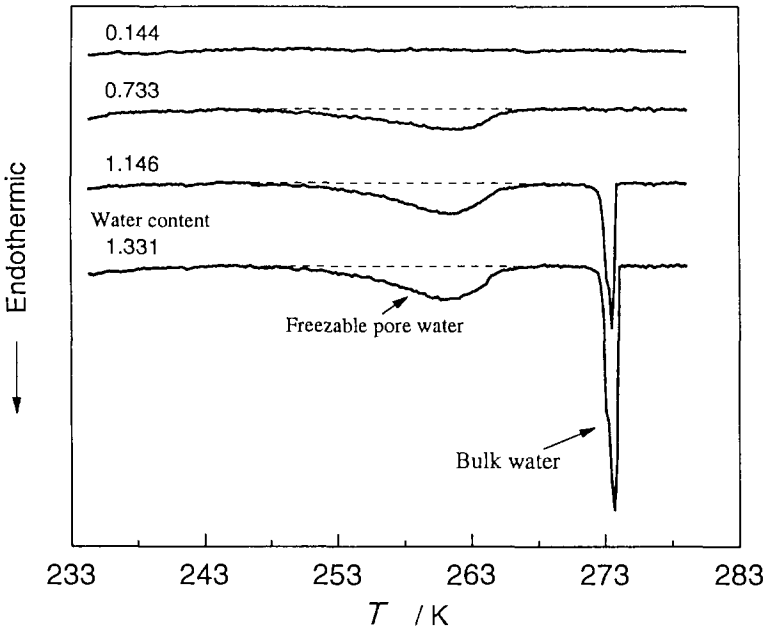

Fig. 3. DSC heating curves of SW27 as a function of water content.

low water content exists only as nonfreezable water. As the water content increases, however, an endothermic peak, which is due to the melting of freezable pore ice in the silica gel, appears within the temperature range up to 273 K. Moreover, an endothermic peak due to the melting of bulk ice overflowing the silica gel appears with increasingly higher water content.

3.2. Determination of bulk water and of freezable and nonfreezable pore water

Bulk water content W_b, freezable pore water content W_{fp}, and nonfreezable pore water content W_{nf}, which are expressed as the mass ratio of each water content to the dry solid, were calculated from the following equations

$$W_b = \int_{T_0}^{>T_0} \frac{\frac{dq}{dt}}{m\Delta H_0} dt \tag{1}$$

$$W_{fp} = \int_{<T_0}^{T_0} \frac{\frac{dq}{dt}}{m\Delta H(T)} dt \tag{2}$$

$$W_{nf} = W_t - W_b - W_{fp} \tag{3}$$

where T_0 is the triple point of water, m is the weight of the silica gel, W_t is the total water content in g of H_2O per g of silica gel measured by the change in mass of the samples before and after drying, and dq/dt represents the heat flow of the DSC signal, ΔH_0 is the enthalpy change at T_0 and $H(T)$ is the enthalpy change of fusion of the ice in J g^{-1} that can be approximately calculated from the following equation of Randall [12,13]

$$\Delta H(T) = 334.1 + 2.119(T - 273.15) - 0.00783(T - 273.15)^2 \quad (4)$$

where T is the temperature in K. Riedel verified the validity of Eq. (4) with measurements of enthalpy using an accurate absolute calorimeter [13].

In addition, the change in freezing and melting enthalpy of ice can also be calculated from Kirchhoff's law

$$\Delta H(T) = \Delta H_0 + \int_{T_0}^{T} [C_{p\,\mathrm{water}}(T) - C_{p\,\mathrm{ice}}(T)]\mathrm{d}T \quad (5)$$

where $C_{p\,\mathrm{water}}(T)$ and $C_{p\,\mathrm{ice}}(T)$ are the heat capacities of water and ice, respectively, as a function of temperature. The $C_{p\,\mathrm{ice}}(T)$ is approximately expressed as a linear function of temperature [14]. On the other hand, that of water increases as the temperature decreases and diverges asymptotically as the temperature approaches 227 K [15–17], and it can be approximately expressed as a function of temperature using a polynomial [17]. The differences between freezable pore water content calculated using Eq. (4) and that obtained by the substitution of Eq. (5) for the $C_{p\,\mathrm{ice}}(T)$, determined by Fukusako, and for the $C_{p\,\mathrm{water}}(T)$, determined by Speedy, were $< 0.3\%$ for SA18 and $< 0.2\%$ for SA75. The differences are thus negligible.

Incidentally, instead of using the $C_{p\,\mathrm{water}}(T)$ proposed by Speedy, a linear function of temperature approximated by the authors regarding the heat capacities of liquid water over the temperature range above 273 K reported by Ginnings and Furukawa [18], $C_{p\,\mathrm{water}}(T) = 75.390 + 2.498 \times 10^{-4}T$, in J g^{-1} K^{-1}, was also extrapolated on the low temperature side for determining the freezable pore water content using Eqs. (2) and (5). As a result, the differences between freezable pore water content calculated using Eq. (4) and that obtained by the substitution of Eq. (5) for the $C_{p\,\mathrm{water}}(T)$ that is expressed as a linear function of temperature were found to be $< 0.5\%$ for SA18 and $< 0.2\%$ for SA75. These differences are thus also negligible. Consequently, as far as these silica gels are concerned, the approximate Eq. (4) can be used satisfactorily instead of Eq. (5) with only slight errors in calculation for determining the freezable pore water content.

Fig. 4 shows W_b, W_{fp} and W_{nf} as a function of the total water content. In any silica gel, as the water content was increased, nonfreezable pore water appeared in DSC curve at first, and then the W_{nf} increased with increasing water content. Subsequently, freezable pore water appeared when the W_{nf} was saturated. As the water content was increased further, the W_{fp} increased, and then bulk water appeared when the W_{fp} reached saturation. Moreover, the bulk water content increased linearly with increasing water content after the amounts of both freezable and nonfreezable pore water had reached saturation. Similar investigations regarding nonfreezable and bulk water have been reported [4,19–21]; however, the

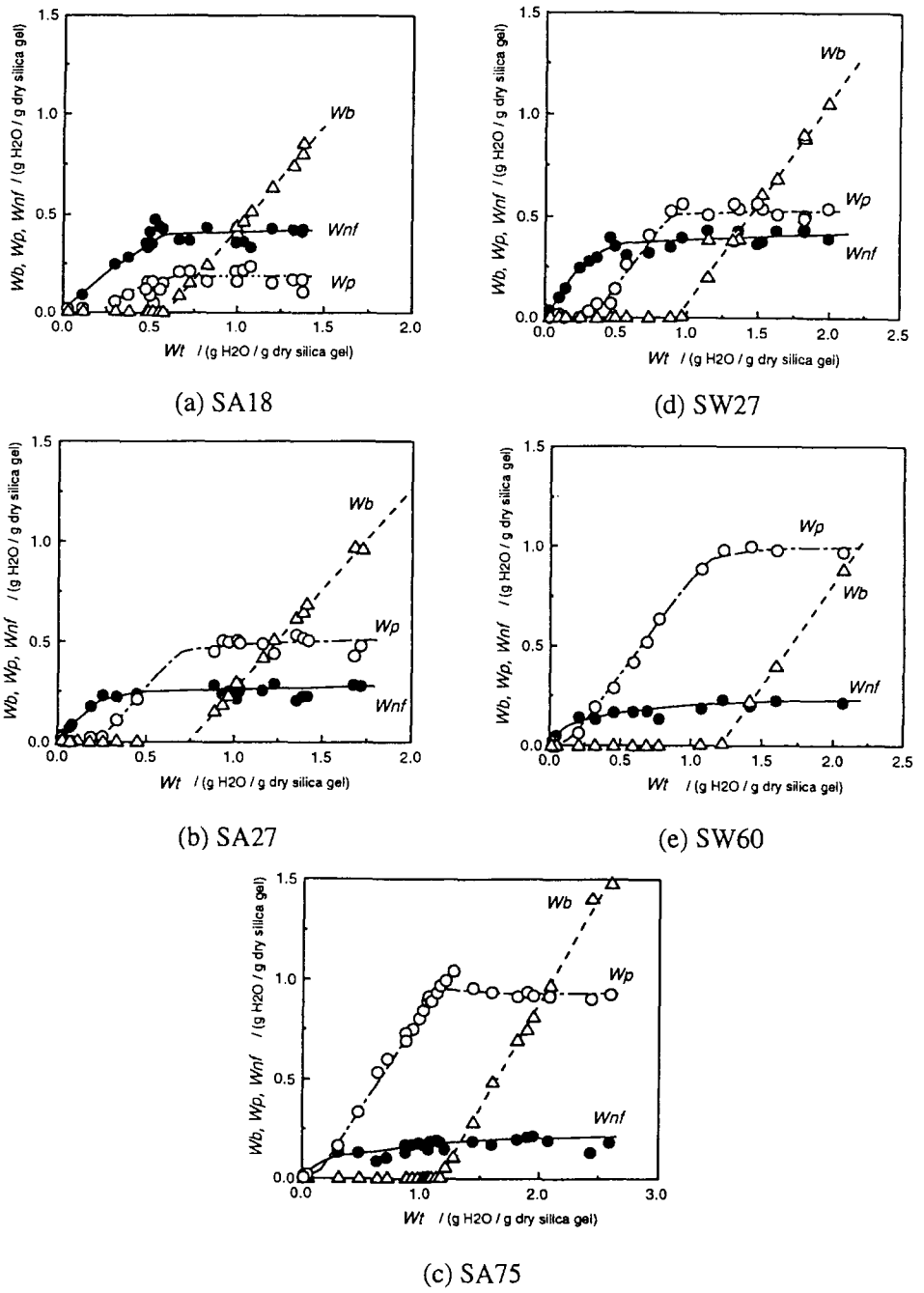

Fig. 4. The amounts of bulk water (W_b; open triangles), freezable pore water (W_{fp}; open circles) and nonfreezable pore water (W_{nf}; closed circles) as a function of total water contents (W_t) in silica gels having various water contents.

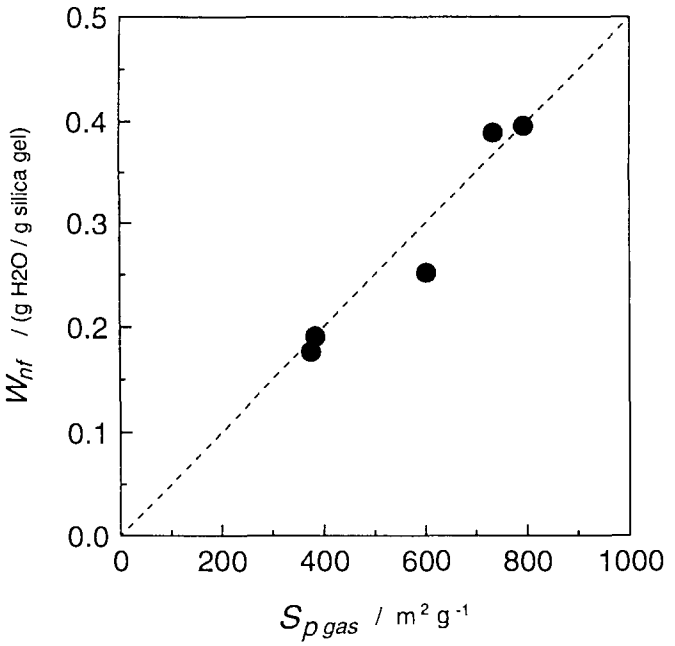

Fig. 5. Comparison of nonfreezable pore water content W_{nf} and specific surface area $S_{p_{gas}}$ obtained using nitrogen gas adsorption–desorption measurement.

dependence of the amount of freezable pore water on the total water content has rarely been reported so far.

Table 2 lists the saturated water contents of freezable and nonfreezable pore water in the silica gels. The saturated freezable pore water contents were found to be larger than the saturated nonfreezable pore water contents in all samples except SA18. Incidentally, the saturated water content of nonfreezable pore water was compared with the surface area of the silica gels as shown in Table 1. The relationship between them is also illustrated in Fig. 5. The nonfreezable water content is found to increase linearly as the surface area is increased. This fact strongly suggests that the nonfreezable pore water exists on the surface of the silica gel; it also suggests that the large value for the saturated nonfreezable pore water content in SA18 can be attributed to the large surface area of the silica gel.

3.3. Determination of pore volume of silica gels

The entire pore volume of silica pores V_{Pdsc} is represented as the sum of the volume occupied by pore water V_{fp} and that occupied by nonfreezable water V_{nf}.

$$V_{Pdsc} = V_{fp} + V_{nf} \tag{6}$$

Each volume can be calculated by dividing the mass by the corresponding density. Because the pore volume may be decreased during melting because of the

smaller specific volume of water than that of ice, on melting of freezable pore ice the V_{fp} must be calculated using the density of freezable pore ice. In contrast, because nonfreezable pore water does not have a phase transition over the temperature range from 233 K to room temperature, V_{nf} can be calculated using the density of nonfreezable water.

Few studies have reported the densities of pore water. Etzler and Fagundus have found that the densities of water confined in the pores of silica gels and porous glasses decrease as the pore radii increase [22,23]. As shown in Table 2, W_{nf} tends to increase due to the increase in the surface area with decreasing pore size. Therefore the depression of the density of pore water in small pore sizes is considered to be reduced by the increase in nonfreezable pore water. In the present work, the density of nonfreezable pore water was assumed to be approximately the same as that of bulk ice at 273.15 K, 0.91671 g cm^{-3}, whereas the density of freezable pore ice was assumed to be the same as the density of bulk water, which is expressed as a function of temperature by the following equation formulated by Fukusako [14]

$$\rho_{\text{freezable pore ice}}(T) = 917.0(1.032 - 1.17 \times 10^{-4}T) \tag{7}$$

where $\rho_{\text{freezable pore ice}}(T)$ is the density of bulk ice in kg cm^{-3} over the temperature range from 133 to 273.15 K and the unit for T is K.

On the basis of these assumptions, V_{fp} and V_{nf} will be given approximately by

$$V_{fp} = \int \frac{\dfrac{dq}{dt}}{\rho_{\text{freezable pore ice}}(T)\Delta H(T)} dt \tag{8}$$

$$V_{nf} = \frac{W_{nf}}{\rho_{\text{nonfreezable pore water}}} \tag{9}$$

The differences between the freezable pore volumes obtained by substitution of Eq. (8) for Eq. (4) and those obtained by substitution of Eq. (8) for Eq. (5), using the $C_{p\,ice}(T)$ of Fukusako and the $C_{p\,water}(T)$ of either Speedy or Ginnings, were $< 0.02\%$ for SA18 as well as SA75. Therefore, as far as these silica gels are concerned, the approximate Eq. (4) can be used satisfactorily with slight errors in calculation for determining the pore volume as well as the amount of the pore water content.

The values of V_{fp}, V_{nf} and V_{Pdsc} are given in Table 2. Furthermore, the relationship between V_{Pdsc} and that obtained from nitrogen gas adsorption–desorption V_{gas}, is illustrated in Fig. 6. The V_{Pdsc} is found to be in notably good agreement with V_{gas}. The differences between V_{Pgas} and V_{Pdsc} ranged from -4 to 8%. Considering that the experimental errors for V_{Pgas} are $\pm 5\%$ and that the value of V_{Pgas} is not necessarily justified because the calculation for V_{Pgas} is based on the assumption that the density of condensed nitrogen gas in a pore is the same as that of bulk nitrogen as liquid at 77 K, the differences between V_{Pgas} and V_{Pdsc} are not significant.

Additionally, in order to confirm the validity of the assumptions, an average density $\rho_{average}$ of the entire pore water after melting at 273 K was calculated using V_{fp} and V_{nf} and the equation

$$\rho_{average} = \frac{\rho_{water}(273\ K)V_{fp} + \rho_{ice}(273\ K)V_{nf}}{V_{pdsc}} \quad (10)$$

where $\rho_{water}(273\ K)$ and $\rho_{ice}(273\ K)$ are the densities of bulk water and bulk ice, respectively. The results for $\rho_{average}$ as a function of the peak radius of the curve of the pore size distribution obtained using nitrogen gas adsorption–desorption are shown in Fig. 7. It is found that the $\rho_{average}$ decreases with decreasing peak radius. The closed and open triangles represent the densities of water in the silica pores at 283 and 293 K, respectively, which were measured by Etzler and Fagundus using a pycnometer. It is clear that their results are consistent with the $\rho_{average}$ calculated using Eq. (10). Consequently, the tendency of the density of pore water to decrease as the pore radius decreases can phenomenologically be explained by the amounts of both V_{nf} and V_p as a function of pore radius. If the densities of both freezable and nonfreezable pore water are the same as that of bulk water, $\rho_{average}$ must be constant at ≈ 1 g cm^{-3}. This suggests that some assumptions in the calculation of the entire pore volume regarding the densities of both freezable pore ice and nonfreezable pore water, and also regarding the heat of melting of the freezable pore water, can be considered to be rational. Namely, the density of freezable pore

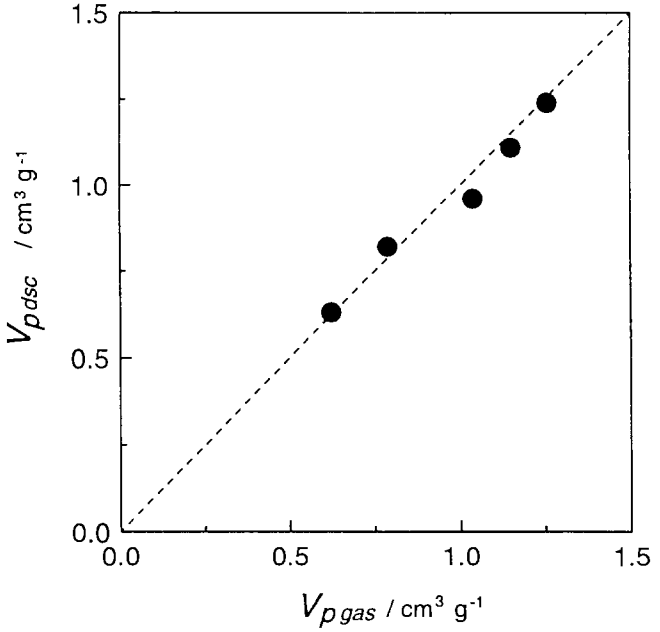

Fig. 6. Comparison of the pore volume obtained using nitrogen gas adsorption–desorption measurement, V_{pgas}, and that obtained using DSC measurement, V_{pdsc}.

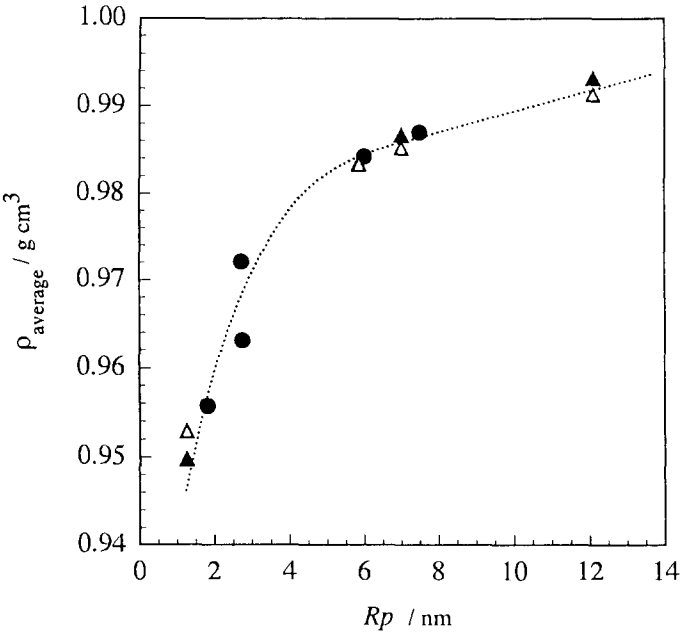

Fig. 7. Average density of pore water calculated from V_{fp} and V_{nf} as a function of peak radius of the PSD_{gas} (closed circles). Closed and open triangles are the densities of water confined in silica pores measured using a pycnometer by Etzler and Fagundus at 283 K and at 293 K, respectively [22].

water will be close to that of bulk water, and the density of nonfreezable pore water will be close to that of bulk ice. On the basis of these assumptions, the pore volume can be determined with sufficient precision in calculations using DSC measurement as well as gas adsorption–desorption measurement.

3.4. Thickness of layer of nonfreezable pore water

Assuming the shape of the silica pores, the thickness β of nonfreezable pore water on the surface can be approximately calculated. Using a shape factor z, which is equal to 2 for a cylindrical pore and 3 for both a circular cone and a spherical pore, the ratio ω of the total volume of the silica pores to that of pore water can be expressed as

$$\omega = \frac{V_{fp} + V_{nf}}{V_{fp}} = \frac{R^z}{r^z} \tag{11}$$

where R is the radius of the pore and r is the radius of freezable pore water which is related to R using β by $R = r + \beta$. By substituting this equation for Eq. (11) and rearranging, one obtains

$$\beta = (1 - \omega^{-1/z})R \tag{12}$$

A monodispersity of pore size distribution, in which all the pores have the same radius R, was assumed to solve Eq. (12). In the present paper, the peak radius $R_{P_{gas}}$ of the distribution curve of the pore sizes obtained using nitrogen gas adsorption–desorption was used for the determination of β. By substitution of $R_{P_{gas}}$ for R of Eq. (14), the thickness of nonfreezable pore water in the silica gels was determined as shown in Table 2. The values of β for all the silica gels are found to range from 0.5 to 0.8 nm in the case of $z = 2$ (cylinder) and from 0.3 to 0.6 nm in the case of $z = 3$ (circular cone or sphere), indicating that the thickness of the layer of nonfreezable bound water corresponds to 1–3 molecules of water from the surface, because the van der Waals radius of water is ≈ 0.3 nm. This finding is similar to the hypotheses of two or three monolayers that have been reported in the literature [4,8,24–26]. As described above, in the present paper, a monodispersity of the distribution of the pore sizes was assumed to calculate β approximately from Eq. (12); however, even if the pore size distribution is considered, the above findings regarding the value of β cannot be disproved [9,10].

Acknowledgment

We acknowledge the support of Atsushi Sakamoto in helping with the nitrogen adsorption–desorption measurements.

References

[1] Y.L. Belorai and E.A. Bylina, Russ. J. Phys. Chem. (Engl. Transl.), 43 (1972) 1698.
[2] Y.J. Iwagnai, J. Chem. Soc. Jpn., 72 (1951) 259.
[3] W.A. Patrick and W.A. Kemper, J. Phys. Chem., 42 (1938) 369.
[4] W. Drost-Hansen, Ind. Eng. Chem., 61 (1969) 10.
[5] G.K. Rennie and J. Clifford, J. Chem. Soc. Faraday Trans. 1, 73 (1977) 680.
[6] W. Drost-Hansen and F.M. Etzler, Langmuir, 5 (1989) 1439.
[7] Y.P. Handa, M. Zakrzewski and C. Fairbridge, J. Phys. Chem., 96 (1992) 8594.
[8] C.L. Jackson and G.B. McKenna, J. Chem. Phys., 93 (1990) 9002.
[9] K. Ishikiriyama, M. Todoki and K. Motomura, J. Colloid Interface Sci., in press.
[10] K. Ishikiriyama and M. Todoki, J. Colloid Interface Sci., in press.
[11] D. Dollimore and G.R. Heal, J. Appl. Chem, 14 (1964) 109.
[12] M. Randall, International Critical Tables. V–VII, McGraw-Hill, New York, 1930.
[13] C.S. Chen, Trans Am. Soc. Agric. Eng., 5 (1988) 1602.
[14] S. Fukusako, Int. J. Thermophys., 11 (1990) 353.
[15] D.H. Rasmussen and A.P. MacKenzie, J. Chem. Phys., 59 (1973) 5003.
[16] C.A. Angell, M. Oguni and W.J. Sichina, J. Phys. Chem., 86 (1982) 998.
[17] R.J. Speedy, J. Phys. Chem., 91 (1987) 3354.
[18] D.C. Ginnings and G.T. Furukawa, J. Am. Chem. Soc., 75 (1953) 522.
[19] T. Hatakeyama, H. Yoshida and H. Hatakeyama, Polymer, 28 (1987) 1282.
[20] H. Yoshida, T. Hatakeyama and H. Hatakeyama, Polymer, 31 (1990) 693.
[21] K. Ishikiriyama and M. Todoki, J. Polym. Sci. B, Polymer Phys., in press.

[22] F.M. Etzler and D.M. Fagundus, J. Colloid Interface Sci., 115 (1972) 513.
[23] F.M. Etzler, Adv. Exp. Med. Biol., 302 (1991) 805.
[24] A.A. Antoniu, J. Phys. Chem., 68 (1964) 2745.
[25] G.G. Litvan, Can. J. Chem., 44 (1966) 2617.
[26] P.A. Theil, Acc. Chem. Res., 24 (1991) 31.